Icarus 206 (2010) 735–746

Contents lists available at ScienceDirect

Icarus

journal homepage: www.elsevier.com/locate/icarus

Fragmentation model dependence of collision cascades

Hiroshi Kobayashi [a,b,*], Hidekazu Tanaka [b]

[a] Astrophysical Institute and University Observatory, Friedrich Schiller University, Schillergaesschen 2-3, 07745 Jena, Germany
[b] Institute of Low Temperature Science, Hokkaido University, Kita-Ku Kita 19 Nishi 8, Sapporo 060-0819, Japan

ARTICLE INFO

Article history:
Received 12 June 2009
Revised 24 September 2009
Accepted 1 October 2009
Available online 13 October 2009

Keywords:
Collisional physics
Asteroids, Dynamics
Planetary dynamics
Planetary formation

ABSTRACT

Mass depletion of bodies through successive collisional disruptions (i.e., collision cascade) is one of the most important processes in the studies of the asteroids belt, the Edgeworth-Kuiper belt, debris disks, and planetary formation. The collisional disruption is divided into two types, i.e., catastrophic disruption and cratering. Although some studies of the collision cascades neglected the effect of cratering, it is unclear which type of disruption makes a dominant contribution to the collision cascades. In the present study, we construct a simple outcome model describing both catastrophic disruption and cratering, which has some parameters characterizing the total ejecta mass, the mass of the largest fragment, and the power-law exponent of the size distribution of fragments. Using this simple outcome model with parameters, we examine the model dependence of the mass depletion time in collision cascades for neglect of coalescence of colliding bodies due to high collisional velocities. We find the cratering collisions are much more effective in collision cascades than collisions with catastrophic disruption in a wide region of the model parameters. It is also found that the mass depletion time in collision cascades is mainly governed by the total ejecta mass and almost insensitive to the mass of the largest fragment and the power-law exponent of fragments for a realistic parameter region. The total ejecta mass is usually determined by the ratio of the impact energy divided by the target mass (i.e. Q-value) to its threshold value $Q_D^\star$ for catastrophic disruption, as well as in our simple model. We derive a mass depletion time in collision cascades, which is determined by $Q_D^\star$ of the high-mass end of collision cascades. The mass depletion time derived with our model would be applicable to debris disks and planetary formation.

1. Introduction

Disruption by successive high-velocity collisions plays an important role in evolution of the asteroid belt (e.g., Bottke et al., 2005), the Edgeworth-Kuiper belt (e.g., Stern and Colwell, 1997; Kenyon and Luu, 1999; Krivov et al., 2005; Kenyon et al., 2008), and debris disks (e.g., Löhne et al., 2008; Kenyon and Bromley, 2004, 2008). The successive collisional disruptions form the so-called "collision cascade". In collision cascades, bodies become smaller and smaller by successive collisions and a (constant) downward mass flux in the mass space is produced (e.g., Tanaka et al., 1996). Very small bodies created in collision cascades are removed by the gas drag in protoplanetary disks, and by the Poynting–Robertson effect, or the radiation pressure in debris disks. The downward mass flux is controlled by disruption of the largest bodies and the depletion rate of the total mass is determined by the mass flux.

Collisional disruption is divided into two categories, i.e., catastrophic disruption and cratering. The cratering is caused by low-energy impacts. The resulting total ejecta mass is much smaller than the mass of the target. In contrast, the catastrophic disruption which occurs in high-energy impacts fully destroys the target. Thus, the total mass of fragments in catastrophic disruption is much larger than that in cratering. However, the cratering caused by small impactors is much more frequent than the catastrophic disruption. Dohnanyi (1969) and Williams and Wetherill (1994) suggested that the effect of cratering is much smaller than catastrophic disruptions, using their collisional outcome model. In most of later analytic studies, the cratering is assumed to be negligible (e.g., O'Brien and Greenberg, 2003; Wyatt et al., 2007). However, it should be noted that the collisional outcome model of Dohnanyi (1969) and Williams and Wetherill (1994) includes a parameter determining the total ejecta mass at a single cratering event. Although the cratering is ineffective in the nominal cases of their papers, this result depends on the parameter. Such a important parameter should be fixed by comparing with results of laboratory experiments and/or hydrodynamic numerical simulations on collisional disruptions. In addition, the contribution of cratering to the mass depletion rate (or mass flux) in collision cascades was not shown in numerical simulations including cratering

* Corresponding author. Address: Astrophysical Institute and University Observatory, Friedrich Schiller University, Schillergaesschen 2-3, 07745 Jena, Germany. Fax: +49 3641 947 532.
E-mail address: hkobayas@astro.uni-jena.de (H. Kobayashi).

0019-1035/$ - see front matter © 2009 Elsevier Inc. All rights reserved.
doi:10.1016/j.icarus.2009.10.004

(e.g., Thébault and Augereau, 2007; Kenyon and Bromley, 2002, 2008; Wetherill and Stewart, 1993; Inaba et al., 2003; Krivov et al., 2008). Hence it is still unclear which type of disruption is dominant in collision cascades.

The properties of collision cascades such as the mass depletion rate is strongly dependent on the outcome model of collision disruption (i.e., the model of the size distribution of fragments created at each collision). This dependence brings a large uncertainty of collision cascades. A simple outcome model of the cratering would be characterized by the total mass of ejecta, the mass of the largest fragment (except for the eroded target) and the power-law exponent of the size distribution of fragments. When the impact energy divided by the target mass (i.e., Q-value) is large enough, the total mass of ejecta is larger than the mass of the eroded target and the disruption mode turns into the catastrophic disruption. The total mass of ejecta determining the disruption mode would also govern the mass depletion rate in collision cascades. On the other hand, it is uncertain how the mass depletion rate depends on the mass of the largest fragment or the power-law exponent. Furthermore, laboratory experiments of collisional disruption showed that collisional outcomes are much more complex. For example, Takagi et al. (1984) showed for catastrophic disruption of basalt targets that the size distribution of fragments is expressed by three power-laws rather than a single power-law. We have to clarify how collision cascades depends on such details of realistic collisional outcomes.

Debris disks observed around main-sequence stars would be formed through collisional disruption of planetesimals. Since the observed small particles are removed in a short timescale, the disruption of planetesimals is expected to be still on-going. The luminosity of a debris disk gives us some information on the total mass of planetesimals and their collision rate. Dominik and Decin (2003) developed a simple analytic model of debris disks and estimated the depletion time of total mass of bodies (or the total mass of dust debris). Wyatt et al. (2007) proposed another analytic model. They took into account the velocity dependence of the depletion time. However, these studies use an extremely simple outcome model. They neglected the contribution of cratering collisions and did not take into account the size distribution of fragments. Due to cratering collisions, the depletion time may be reduced significantly. Hence, using more realistic outcome model, we should revise their simple analytical model on the depletion time.

The collisional disruption is also important in the planet formation process. Planetary embryos are formed through accretion of planetesimals. The embryos enhance the relative velocities between planetesimals by their strong gravity. Inaba et al. (2003) showed that collisional disruption of planetesimals is dominant rather than their coalescence when embryos are Mars-size or larger. The mass depletion of planetesimals due to disruption would slow down the growth of planetary embryos. Thus, the accurate mass depletion time of planetesimals is also required in the study of planetary growth.

In the present study, we examine the dependence of collision cascades on the outcome model of collisional disruption. To do so, we first construct a simple outcome model describing both catastrophic disruption and cratering. In our model, outcome is characterized by the total ejecta mass, the mass of the largest fragment, and the power-law exponent of the size distribution of fragments with some parameters. With this simple outcome model, we clarify how the cratering collisions affect the mass depletion time in collision cascades and how the mass depletion time depends on details of the outcome model.

In Section 2, we describe basic equations governing evolution of the mass distribution due to disruption. In Section 3, we explain our outcome model of collisional disruption. In Section 4, assuming self-similar collision cascades, we analytically derive the mass flux in the mass space of collision cascades. We will show that the cratering makes a dominant contribution to the mass flux compared with the catastrophic disruption. In Section 5, we also derive a simple formula of the mass depletion time and compare it with that in the previous studies. In Section 6, we check our analytical formula, by comparing with the numerical calculations. In Section 7, we further consider a non-self-similar case. We will find more general expressions of the mass depletion time in the non-self-similar case. In Section 8, using the obtained mass depletion time, we discuss the brightness evolution of debris disks due to collision cascades and examine the depletion of planetesimals due to collisional disruption and its effect on the planet growth. In the final section, we summarize our results.

2. Basic equation

The mass distribution of bodies orbiting in a narrow annulus around a central star evolves with their collisional disruption and/or coalescence. The evolution is governed by the mass conservation law,

$$\frac{\partial m n_s(m)}{\partial t} + \frac{\partial F(m)}{\partial m} = 0, \tag{1}$$

where $n_s(m)dm$ is the surface number density of bodies with masses ranging from m to $m + dm$ and $F(m)$ is the mass flux across mass m. Eq. (1) is valid if there is no removal of bodies from the annulus by gas drag, Poynting–Robertson effect, and radiation pressure. The mass flax $F(m)$ is caused by collisions between bodies. Therefore, $F(m)$ is proportional to the collisional frequency. The collisional frequency between bodies with masses ranging from m_1 to $m_1 + dm_1$ and those from m_2 to $m_2 + dm_2$ in unit area is given by (see Inaba et al., 2001)

$$\Omega_K n_s(m_1) dm_1 n_s(m) dm_2 P_{col}, \tag{2}$$

where Ω_K is the Keplarian angular velocity at the annulus and P_{col} is the collision rate between two bodies with masses m_1 and m_2, which has a dimension of area. Inaba et al. (2001) also defined P_{col} in a similar way but they defined P_{col} as a non-dimensional quantity, by dividing it by the square of the Hill radius.

The collision rate P_{col} is approximately estimated in the following way. In the present paper, we consider only the case where disruption is dominant and neglect coalescence of bodies. This corresponds to the case of high-velocity impacts. In this case, the gravitational focusing effect is also negligible and the collisional cross section σ_{col} is given by the geometrical one. On the other hand, the mean collision time of the species 1 with 2 is inversely proportional to the optical depth of the species 2 defined by $\sigma_{col} n_s(m_2) dm_2$. Since the mean collision time is $\sim 1/\Omega_K$ when the optical depth is unity, the mean collision time is given by $1/[\Omega_K \sigma_{col} n_s(m_2) dm_2]$. Furthermore, noting that the collisional frequency between species 1 and 2 in unit area is equal to the surface number density of the species 1 divided by the collision time of the species 1 with 2, and comparing it with Eq. (2), we obtain $P_{col} \simeq \sigma_{col} \simeq \pi(r_1 + r_2)^2$.

The more exact expression of P_{col} is derived by Greenzweig and Lissauer (1992) or Inaba et al. (2001), by including the three bodies effect, too. When the gravitational focusing is negligible, P_{col} is given by

$$P_{col} = \pi(r_1 + r_2)^2 \frac{\mathscr{F}(I)}{2\pi^2} = h_0 m_1^{\frac{2}{3}} \left(1 + y^{\frac{1}{3}}\right)^2 \tag{3}$$

with

$$h_0 = 6.1 \times 10^{-2} \mathscr{F}(I) \rho^{-\frac{2}{3}}, \tag{4}$$

where $y = m_2/m_1$, I is the ratio of the relative inclination between the colliding bodies to the relative eccentricity, and ρ is the material

density of the colliding bodies. In many cases, the ratio I is assumed to be 0.5 and $\mathscr{F}(I)$ equals 17.3 (Greenzweig and Lissauer, 1992). We also adopt this assumption in the present paper. Then the correction factor $\mathscr{F}(I)/(2\pi^2)$ in Eq. (3) is calculated as 0.88, which indicates that the above approximate expression agrees with the exact one only with the error of ~10%.

To describe the mass distribution of fragments created at a collision of two bodies with masses of m_1 and m_2, Tanaka et al. (1996) introduced a function $f(m, m_1, m_2)$, which is the mass fraction of the fragments that are ejected from the body m_1 and smaller than the mass m. Note that the fragments ejected from the body m_1 and those from the body m_2 are described separately in their formulation with $f(m, m_1, m_2)$. The total of the fragments smaller than m created by the collision is given by

$$m_1 f(m, m_1, m_2) + m_2 f(m, m_2, m_1), \tag{5}$$

and the number of the fragments with masses from m to $m + dm$ created at the collision (denoted by $n_{\rm eject}(m)dm$) is given by

$$\frac{1}{m}\frac{\partial}{\partial m}[m_1 f(m, m_1, m_2) + m_2 f(m, m_2, m_1)]dm. \tag{6}$$

If the function $f(m, m_1, m_2)$ has a power-law dependence as $f(m, m_1, m_2) \propto m^{-q}$ for small fragments, the differential mass distribution function is proportional to m^{-q-2}.

When the coalescence of bodies is negligible because of high-velocity impacts, we have for the (downward) mass flux (see Tanaka et al., 1996)

$$F(m) = -\int_m^\infty dm_1 \int_0^\infty dm_2 \; \Omega_{\rm K} m_1 f(m, m_1, m_2) P_{\rm col} n_{\rm s}(m_1) n_{\rm s}(m_2). \tag{7}$$

Since the integrand on the r.h.s. of Eq. (7) represents the mass flux coming from only m_1, the upper and lower limits of integral over m_2 should be the minimum mass and the maximum mass, respectively. The upper and lower limits can be assuming 0 and ∞ when m is much smaller (larger) than the maximum (minimum) mass (see Appendixes in Tanaka et al., 1996). Eq. (1) with Eq. (7) describes the evolution of the mass distribution of bodies by collisional disruption. To integrate Eq. (7), we need an explicit form of the function $f(m, m_1, m_2)$, which is dependent on the outcome model of collisional disruption.

3. Fragmentation model

We construct a simple model of collisional outcomes which has some parameters. Changing the parameters in the model, we will examine the dependence of properties of collision cascades on the outcome model. Our outcome model gives the explicit form of the function $f(m, m_1, m_2)$, which describes the mass distribution of fragments created at a collision between bodies with masses m_1 and m_2. We recall again that $f(m, m_1, m_2)$ describes only the fragments coming from the body 1 and that the fragments created by a collision between m_1 and m_2 is given by Eq. (5).

Fig. 1 shows the mass distribution of fragments originated from the body 1 by a collision with the body 2 in our outcome model. The mass distribution consists of two parts, i.e., a power-law distribution of small fragments and one large remnant body. The power-law distribution is characterized by three quantities, the total mass of fragments (or ejecta), $m_{\rm e}$, the mass of the largest fragment (except for the remnant body), $m_{\rm L}$, and the power-law exponent, b. The mass of the remnant body is given by $m_1 - m_{\rm e}$. The mass distribution is fixed by these three quantities in our simple model.

In cratering collisions, the total mass of ejecta $m_{\rm e}$ is much smaller than m_1 and increases with the impact energy. When $m_{\rm e}$ is larger than the half of m_1, the disruption mode turns into catastrophic

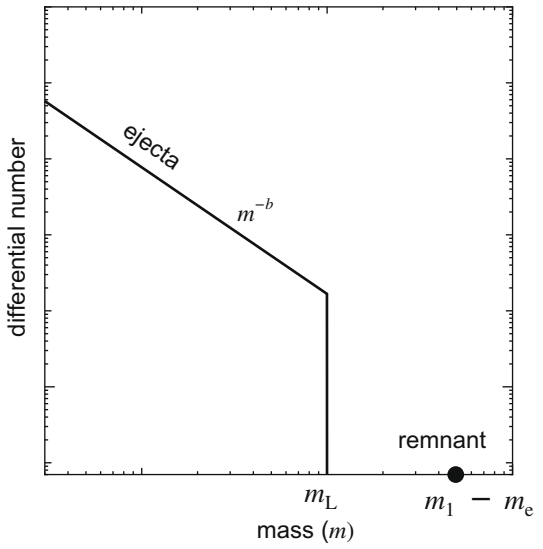

Fig. 1. The differential mass distribution of ejecta yielded from a body m_1 by a collision between bodies of m_1 and m_2 as a function of mass m. For $m < m_{\rm L}$, the differential mass distribution of ejecta is proportional to m^{-b}. The circle indicates the mass of the remnant body with $m_1 - m_{\rm e}$.

disruption. By taking into account such a dependence of $m_{\rm e}$ on the impact energy properly, we can describe outcomes of both cratering and catastrophic disruption with our model.

The disruption mode would also be dependent on the strength of the colliding bodies. We introduce a normalized impact energy ϕ defined by

$$\phi(y) = \frac{E_{\rm imp}}{m_1 Q_{\rm D}^\star} = \frac{v^2}{2Q_{\rm D}^\star}\frac{y}{1+y}, \tag{8}$$

where

$$E_{\rm imp} = \frac{1}{2}\frac{m_1 m_2}{m_1 + m_2} v^2 \tag{9}$$

is the impact energy at the collision between m_1 and m_2 with the velocity v and $Q_{\rm D}^\star$ is the threshold value of the impact energy per unit target mass for catastrophic disruption. In our model, using the normalized impact energy, $m_{\rm e}$ is given by

$$m_{\rm e} = \frac{\phi}{1+\phi} m_1. \tag{10}$$

At a cratering collision with small ϕ, the total ejecta mass $m_{\rm e}$ is proportional to ϕ. At a catastrophic collision with large ϕ, $m_{\rm e}$ is almost equal to m_1 (see Fig. 2). At $\phi = 1$, $m_{\rm e}$ is equal to the mass of the remnant body and $m_1/2$, which is consistent with the definition of $Q_{\rm D}^\star$. It should be noted that we choose a smooth function for $m_{\rm e}/m_1$ to connect the limits of cratering and catastrophic. If the function is not necessary to be smooth, we can set another simple function as $m_{\rm e}/m_1 = \phi/2$ for $\phi < 2$, $m_{\rm e}/m_1 = 1$ for $\phi \geq 2$. Although both satisfy laboratory experiences and fluid dynamical simulations, there is a discrepancy by a factor of 2 between them in the limit of $\phi \ll 1$ (cratering). Thus, there is still uncertainty about a modeling of the total ejecta mass. Since a smooth function of $m_{\rm e}/m_1$ seems natural, we apply Eq. (10) for $m_{\rm e}/m_1$ in this paper.

The high-mass end of the power-law distribution, $m_{\rm L}$, is given in our model by

$$m_{\rm L} = \frac{\epsilon}{1+\phi} m_{\rm e} = \frac{\epsilon\phi}{(1+\phi)^2} m_1, \tag{11}$$

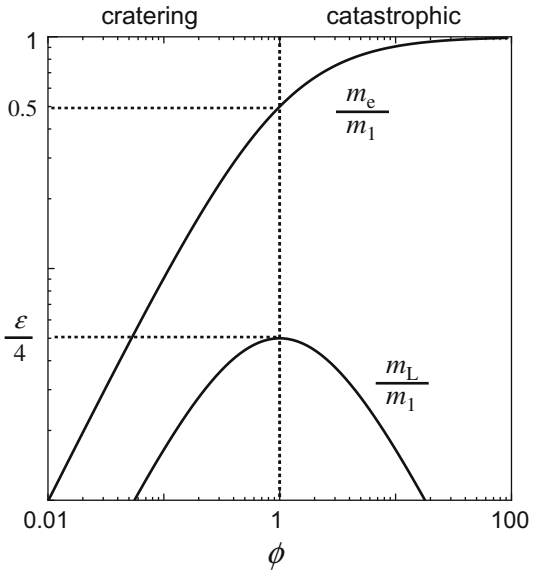

Fig. 2. The total ejecta mass m_e and largest ejecta mass m_L from the body m_1 as functions of the scaled impact energy ϕ in our model. A cratering collision occurs for $\phi \ll 1$ and a catastrophic collision occurs for $\phi \gg 1$.

where ϵ is a non-dimensional parameter (see Fig. 2).[1] For $\phi \ll 1$, m_L is proportional to ϕ while m_L is proportional to $1/\phi$ for $\phi \gg 1$. The energy dependence for $\phi \gg 1$ are consistent with laboratory experiments (e.g., Paolicchi et al., 1996; Arakawa, 1999).

Using this model of the mass distribution of fragments, we can obtain the explicit form of the function $f(m, m_1, m_2)$. We divide the function $f(m, m_1, m_2)$ into two components as $f(m, m_1, m_2) = f_{\rm eject}(m, m_1, m_2) + f_{\rm rem}(m, m_1, m_2)$, where $f_{\rm eject}$ and $f_{\rm rem}$ are the mass fraction functions due to the ejecta and the remnant, respectively. Using the mass distribution described in Fig. 1 with m_e, m_L, and b, we have for $f_{\rm eject}$ and $f_{\rm rem}$

$$m_1 f_{\rm eject}(m, m_1, m_2) = \begin{cases} m_e & (m > m_L), \\ m_e \left(\frac{m}{m_L}\right)^{2-b} & (m \leqslant m_L), \end{cases} \tag{12}$$

and

$$m_1 f_{\rm rem}(m, m_1, m_2) = \begin{cases} m_1 - m_e & (m \geqslant m_1 - m_e), \\ 0 & (m < m_1 - m_e). \end{cases} \tag{13}$$

This outcome model gives the function $f(m, m_1, m_2)$ (or the mass distribution of fragments created at a collision of bodies 1 and 2) for all impact energies or for all mass ratios m_2/m_1. It should be noticed that, in the case of $m_2/m_1 > 1$, the function $f(m, m_1, m_2)$ describes the disruption of the small projectile at a collision with a large target.

Our outcome model has three non-dimensional parameters, i.e., b, ϵ, and the ratio, $v^2/Q_D^\star$. By changing these parameters, we examine the dependence of collision cascades on the outcome model. We adopt the following realistic parameter range in the present paper. According to the laboratory experiments of collisional disruption, the total mass of fragments is determined by the high-mass end of the mass distribution while the total number is governed by the very small fragments. Thus the power-law exponent should be in the range of $1 < b < 2$. The parameter ϵ is related to the high-mass end of the power-law distribution. Since the largest fragment in the power-law distribution should be less massive than the total mass of the distribution m_e, we set $\epsilon < 1$. Next we estimate the value of the ratio $v^2/Q_D^\star$. The collision velocity v is approximately given by $e v_K$, where e is the orbital eccentricity of the colliding bodies and v_K is the Keplarian velocity. Then we have for $v^2/Q_D^\star$

$$\frac{v^2}{Q_D^\star} \sim 2 \times 10^2 \left(\frac{e}{0.1}\right)^2 \left(\frac{a}{50\ {\rm AU}}\right)^{-1} \left(\frac{M_\star}{M_\odot}\right) \left(\frac{Q_D^\star}{10^7\ {\rm erg/g}}\right)^{-1}, \tag{14}$$

where a is the semimajor axis of bodies, $M_\star$ is a mass of the central star, and $M_\odot$ is the solar mass. From Eq. (14), we can estimate the ratio to be $v^2/Q_D^\star = 10^3$–10^4 in the asteroid belt (2–3 AU) and $v^2/Q_D^\star = 10^2$–10^3 in the Edgeworth-Kuiper belt (40–50 AU). Since the eccentricity would be dependent on the masses of planets perturbing colliding bodies and the separations between the bodies and the planets, the eccentricity can be much less than 0.1 in both debris disks and protoplanetary disks. In this paper, therefore, we set the range of $v^2/Q_D^\star$ to be from 10^{-1} to 10^5.

The collisional outcome model of Dohnanyi (1969) and Williams and Wetherill (1994) has a free parameter determining the total ejecta mass at a single cratering event. In our model, on the other hand, the total ejecta mass at a single collision event continuously decreases at the transition from catastrophic disruption to cratering (i.e., at $\phi = 1$). If we include a large discontinuous decrease in the total ejecta mass at the transition, it would significantly reduce the effect of cratering. In most of laboratory experiments and hydrodynamic numerical simulations on collisional disruptions, however, such a discontinuous decrease in the total ejecta mass is not observed (e.g., Housen et al., 1991; Takagi et al., 1984; Benz and Asphaug, 1999). In order to develop a simple and realistic collision outcome model, we do not include such a jump in the total ejecta mass.

4. Mass flux

When the non-dimensional parameters $v^2/Q_D^\star$, ϵ, and b are independent of the masses of the colliding bodies, m_1 and m_2, the function $f(m, m_1, m_2)$ given by Eqs. (10) and (11) depends on only the mass ratios and it is independent of the absolute value of the masses. Namely,

$$f(m, m_1, m_2) = f\left(\frac{m}{m_1}, \frac{m_2}{m_1}\right). \tag{15}$$

For such a self-similar outcome model, a collision cascade has a single power-law size distribution, as seen below (or see Tanaka et al., 1996). In Sections 4–6, we mainly examine this self-similar case. We will show the ratio $v^2/Q_D^\star$ is important in collision cascades compared with other two parameters. In realistic systems, $v^2/Q_D^\star$ is dependent of the masses of the colliding bodies. In Section 7, we also examine the non-self-similar case.

Size distribution of the self-similar collision cascades is obtained as follows. Introducing the non-dimensional variables $x = m/m_1$ and $y = m_2/m_1$, and setting the mass distribution to be $n_s(m) = Am^{-\alpha}$, we can rewrite Eq. (7) as

$$F(m) = -A^2 \Omega_K h_0\ m^{\frac{11}{3}-2\alpha} \int_0^1 dx \int_0^\infty dy y^{-\alpha} \left(1 + y^{\frac{1}{3}}\right)^2 x^{2\alpha-\frac{14}{3}} f(x, y). \tag{16}$$

For a steady state $\partial F(m)/\partial m = 0$, we have (e.g., Dohnanyi, 1969; Tanaka et al., 1996)

$$\alpha = \frac{11}{6}. \tag{17}$$

[1] ϵ is related to b for the identical power-law mass distribution of ejecta even around m_L (e.g., Williams and Wetherill, 1994; O'Brien and Greenberg, 2003). However, since the index b changes with ejecta mass (Takagi et al., 1984), there is uncertainty for the identical power-law distribution. Therefore, we treat ϵ as an independent parameter in this paper.

We examine the (downward) mass flux of the self-similar collision cascades with the power-law exponent of Eq. (17). Since the function f consists of two components, the mass flux $F(m)$ is also divided into two corresponding components, the mass fluxes by ejecta and by the eroded remnant, $F_{\rm eject}$ and $F_{\rm rem}$. The downward fluxes $F_{\rm eject}$ and $F_{\rm rem}$ are produced by ejecta from the body m_1 and by the body m_1 being eroded down to smaller mass, respectively. The flux is given by

$$F(m) = F_{\rm eject}(m) + F_{\rm rem}(m), \tag{18}$$

where

$$F_{\rm eject}(m) = -A^2\Omega_{\rm k}h_0\int_0^\infty dy\frac{y^{-\alpha}\left(1+y^{\frac{1}{3}}\right)^2\phi(y)}{1+\phi(y)} \times\left\{\int_0^{k(y)}x^{2\alpha-\frac{14}{3}}\left[\frac{x}{k(y)}\right]^{2-b}dx+\int_{k(y)}^1 x^{2\alpha-\frac{14}{3}}\,dx\right\}, \tag{19}$$

$$F_{\rm rem}(m) = -A^2\Omega_{\rm k}h_0\int_0^\infty dy\frac{y^{-\alpha}\left(1+y^{\frac{1}{3}}\right)^2}{1+\phi(y)}\int_{\frac{1}{1+\phi(y)}}^1 x^{2\alpha-\frac{14}{3}}\,dx \tag{20}$$

with $k(y)=\epsilon\phi(y)/[1+\phi(y)]^2$. Furthermore, noting that $\alpha = 11/6$ and integrating them over x, we obtain the expression of $F_{\rm eject}$ and $F_{\rm rem}$ as

$$F_{\rm eject}(m) = -A^2\Omega_{\rm K}h_0\int_0^\infty dy\frac{y^{-\alpha}\left(1+y^{\frac{1}{3}}\right)^2\phi(y)}{1+\phi(y)} \times\left[-\ln\frac{\epsilon\phi(y)}{[1+\phi(y)]^2}+\frac{1}{2-b}\right], \tag{21}$$

$$F_{\rm rem}(m) = -A^2\Omega_{\rm K}h_0\int_0^\infty dy\frac{y^{-\alpha}\left(1+y^{\frac{1}{3}}\right)^2}{1+\phi(y)}\ln(1+\phi(y)). \tag{22}$$

In Fig. 3, we show F, $F_{\rm eject}$, and $F_{\rm rem}$ as a function of $v^2/Q_{\rm D}^\star$. For all values of $v^2/Q_{\rm D}^\star$, $F_{\rm rem}$ is smaller than $F_{\rm eject}$ by the factor 10. Since the mass flux is determined by the component $F_{\rm eject}$ of Eq. (21), we readily see that the mass flux F is proportional to $\left(v^2/Q_{\rm D}^\star\right)\ln\left(v^2/Q_{\rm D}^\star\right)$ in the case of $v^2/Q_{\rm D}^\star \ll 1$ and that it is proportional to $\left(v^2/Q_{\rm D}^\star\right)^{\alpha-1}$ for $v^2/Q_{\rm D}^\star \gg 1$. In Fig. 4, we show the dependence of F on the parameters ϵ and b. The flux is insensitive to b and ϵ. This means that the collision cascade is hardly influenced by the high-mass end $m_{\rm L}$ of ejecta and the power-law exponent in the collisional outcome. The important factor is the total mass of ejecta $m_{\rm e}$, which is governed by the ratio $v^2/Q_{\rm D}^\star$.

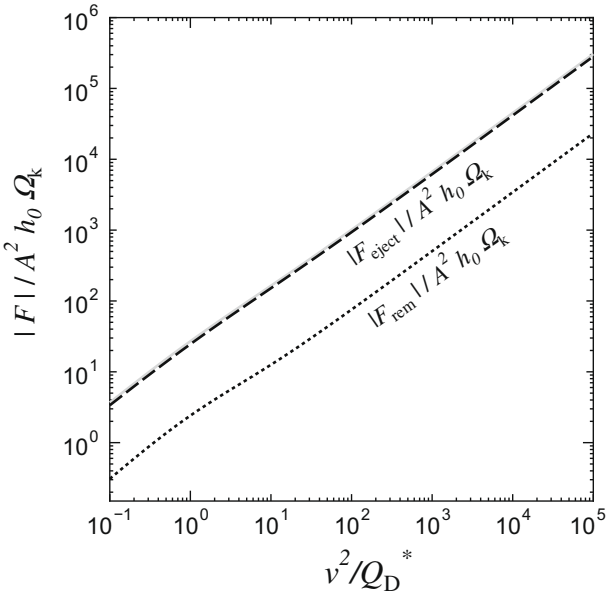

Fig. 3. $F_{\rm eject}$ (dashed lines), $F_{\rm rem}$ (dotted lines), and $F(m) = F_{\rm eject} + F_{\rm rem}(m)$ (gray line) as functions of $v^2/Q_{\rm D}^\star$ for $b = 5/3$ and $\epsilon = 0.2$.

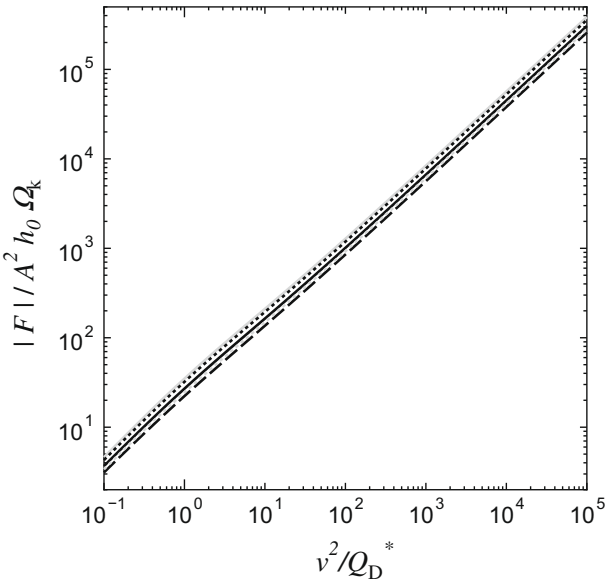

Fig. 4. The dependence of F (Eq. (18) with Eqs. (21) and (22)) on b and ϵ. Here we set $(b,\epsilon) = (5/3, 0.2)$ (solid line), $(1.8, 0.2)$ (dotted lines), $(1.2, 0.2)$ (dashed lines), $(5/3, 0.01)$ (gray solid line), $(5/3, 0.5)$ (gray dotted lines).

Next we compare the contribution of cratering in the flux with that of catastrophic disruption. To do so, we introduce the partial mass flux $F'(m,y')$, which is the contribution of collisions with the mass ratio $y = m_2/m_1$ less than y'. That is, the partial mass flux $F'(m,y')$ is given by

$$F'(m,y') = F'_{\rm eject}(m,y') + F'_{\rm ero}(m,y'), \tag{23}$$

where

$$F'_{\rm eject}(m,y') = -A^2\Omega_{\rm k}h_0\int_0^{y'} dy\frac{y^{-\alpha}\left(1+y^{\frac{1}{3}}\right)^2\phi(y)}{1+\phi(y)} \times\left[-\ln\frac{\epsilon\phi(y)}{[1+\phi(y)]^2}+\frac{1}{2-b}\right], \tag{24}$$

$$F'_{\rm rem}(m,y') = -A^2\Omega_{\rm k}h_0\int_0^{y'} dy\frac{y^{-\alpha}\left(1+y^{\frac{1}{3}}\right)^2}{1+\phi(y)}\ln(1+\phi(y)).$$

From this definition, we have $F'(m,\infty) = F(m)$. In Fig. 5, we show the y-dependence of the partial mass flux $F'(m,y)$. Cratering collisions and catastrophic collisions are distinguished by the value of ϕ which is determined by y. In Fig. 5, we used black lines for the region of cratering collisions and gray lines for catastrophic collisions. According to the usual definition, the high-y case belongs to cratering collisions as well as the low-y case and we adopt it in Fig. 5. For $v^2/Q_{\rm D}^\star = 2$ (or less), all collisions are cratering and, obviously, the mass flux is determined by cratering collisions. In the high-velocity cases with $v^2/Q_{\rm D}^\star = 200$ or 20,000, catastrophic disruption occurs at collisions with an intermediate mass ratio y. We see that the contribution of cratering collisions is about 10 times as large as that of catastrophic collisions even in these high-velocity cases. The importance of cratering collisions are explained by their high-frequency. In Fig. 6, we plot $dF'(m,y)/d\ln y$ as a function of y. This is given by the integrand of Eqs. (21) and (22) multiplied by y. This figure also indicates the importance of cratering collisions. The function

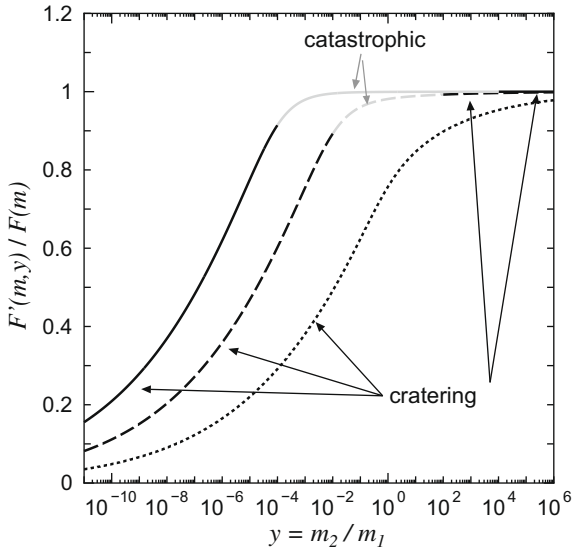

Fig. 5. The partial mass flux $F'(m,y)$ in Eq. (23) scaled by the total mass flux $F(m)$ in Eq. (18) with Eqs. (21) and (22) as a function of y for $v^2/Q_D^\star$ = 20,000 (solid line), 200 (dashed lines), and 2 (dotted lines).

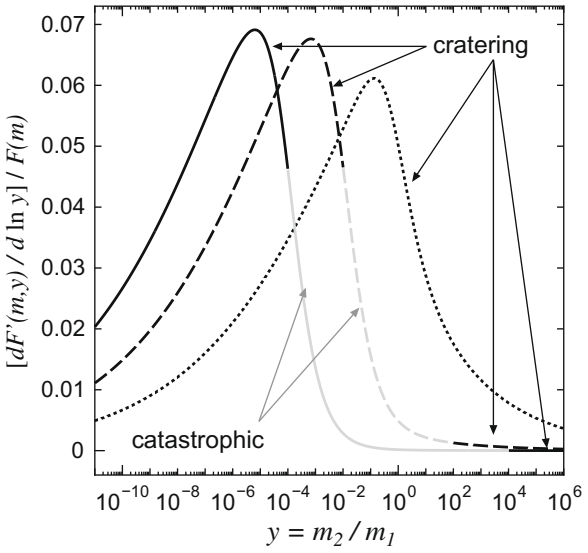

Fig. 6. $[dF'(m,y')/d\ln y']/F(m)$ as a function of y' for $v^2/Q_D^\star$ = 20,000 (solid line), 200 (dashed lines), and 2 (dotted lines).

$dF'(m,y)/d\ln y$ has a peak in the region of cratering collisions and it is not negligible even at collisions with very small mass ratios of $y = 10^{-8}$ because of its weak dependence on y ($\propto y^{1/6}$). We also checked that the importance of cratering collisions is almost independent of the parameters ϵ and b.

In the case of $v^2/Q_D^\star \gg 1$, we can simplify the integrals in Eqs. (21) and (22) using the fact that the contribution of collisions with $y \ll 1$ is dominant in this case (see Fig. 5). Since $v^2/Q_D^\star$ is large in the asteroid belt or in debris disks, this approximation is valid. As a result, we obtain for $v^2/Q_D^\star \gg 1$ (see Appendix A for a derivation)

$$F(m) = -A^2\Omega_k h_0 \left(\frac{v^2}{2Q_D^\star}\right)^{\frac{5}{6}} \left[\left(-\ln\epsilon + \frac{1}{2-b}\right)s_1 + s_2 + s_3\right]. \tag{25}$$

For $\alpha = 11/6$, $s_1 \simeq 6.3$, $s_2 \simeq 38.1$, and $s_3 \simeq 5.6$ (see Appendix A). The results on the mass flux obtained above are seen in Eq. (25), too. The term s_3 in Eq. (25) comes from the $F_{\rm rem}$ while the terms s_1 and s_2 correspond to $F_{\rm eject}$. Since $s_2 \ll s_3$, $F_{\rm eject}$ is much larger than $F_{\rm rem}$. Furthermore, we can understand the insensitivity of F on b and ϵ from $s_2 \gg s_1$ in Eq. (25).

5. Mass depletion time

We consider the mass depletion in collision cascades. In a collision cascade, large bodies near high-mass end have most of the total mass. Their mass gradually decreases due to the downward mass flux of the collision cascade. Although the mass flux produces a large amount of small fragments, these fragments would finally be removed by the gas drag, the Poynting–Robertson, or the radiation pressure at low-mass end. Using the (negative) downward mass flux in unit area, F, the evolution of the total surface density is given by

$$\frac{d\Sigma}{dt} = F(m). \tag{26}$$

Note that the mass flux $F(m)$ is independent of m in a wide mass range between the high- and low-mass ends of steady collision cascades. The constant mass flux $F(m)$ is given by Eq. (18) with Eqs. (21) and (22). On the other hand, the total surface density is given by

$$\Sigma = \int_{m_{\rm min}}^{m_{\rm max}} m n_s dm = \frac{m_{\rm max}^{2-\alpha}}{2-\alpha} A. \tag{27}$$

Exactly speaking, the power-law mass distribution used above is not valid near the high-mass end $m_{\rm max}$. Thus Eq. (27) is an approximate equation. The validity of Eq. (27) will be checked in the next section with numerical simulations of collision cascades. From Eqs. (18), (21), (22), (26), and (27), we obtain a differential equation of the coefficient A. Solving it, we have for $\Sigma(t)$

$$\Sigma(t) = \frac{\Sigma_0}{1 + t/\tau_{\rm dep}}, \tag{28}$$

where Σ_0 is the initial surface density and $\tau_{\rm dep}$ is the so-called mass depletion time of the collision cascade given by

$$\tau_{\rm dep}^{-1} = \frac{1}{36}\Omega_K \frac{\Sigma_0}{m_{\rm max}} h_0 m_{\rm max}^{\frac{2}{3}} \times \left\{ \int_0^\infty dy \frac{y^{-\alpha}\left(1+y^{\frac{1}{3}}\right)^2 \phi(y)}{1+\phi(y)} \left[-\ln\left(\frac{\epsilon\phi(y)}{[1+\phi(y)]^2}\right) + \frac{1}{2-b}\right] + \int_0^\infty dy \frac{y^{-\alpha}\left(1+y^{\frac{1}{3}}\right)^2}{1+\phi(y)} \ln(1+\phi(y)) \right\}. \tag{29}$$

Roughly speaking, $\Sigma_0/m_{\rm max}$ is the surface number density of bodies with $\sim m_{\rm max}$ and $h_0 m_{\rm max}^{2/3}$ is their $P_{\rm col}$ (see Eq. (3)). Hence the term of $\left[\Omega_K(\Sigma_0/m_{\rm max})h_0 m_{\rm max}^{2/3}\right]^{-1}$ in Eq. (29) is approximately equal to the collisional time of bodies with $\sim m_{\rm max}$ (see Eq. (2)). Note that $\tau_{\rm dep}$ defined in Eq. (29) corresponds to the depletion time in the initial depletion stage. To estimate the depletion time scale for strongly depleted disks, we should replace Σ_0 by $\Sigma(t)$ (i.e., the depleted surface density) in Eq. (29).

As well as the mass flux, the mass depletion time has only a weak dependence on the parameters ϵ and b and it is almost governed by the ratio $v^2/Q_D^\star$ (see Fig. 4). Thus the mass depletion time hardly depends on the exponent b and the high-mass end m_L of the mass distribution in the outcome model. As seen in the mass flux, furthermore, the mass depletion time is almost determined by cratering collisions and the contribution of catastrophic collisions is minor.

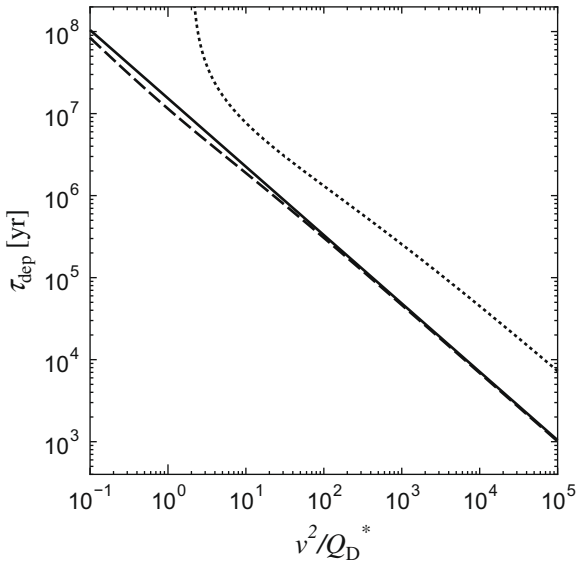

Fig. 7. The mass depletion time τ_{dep} due to collision cascades as a function of $v^2/Q_D^\star$ for $M_{total} = M_\oplus$, $a = 2.5$ AU, $\Delta a = 1$ AU, $m_{max} = 1.3 \times 10^{22}$ g, $\rho = 3$ g cm^{-3}. Solid, dashed, and dotted lines indicate τ_{dep} in Eq. (30) for high-velocities, that in Eq. (29), that derived by Wyatt et al. (2007), respectively.

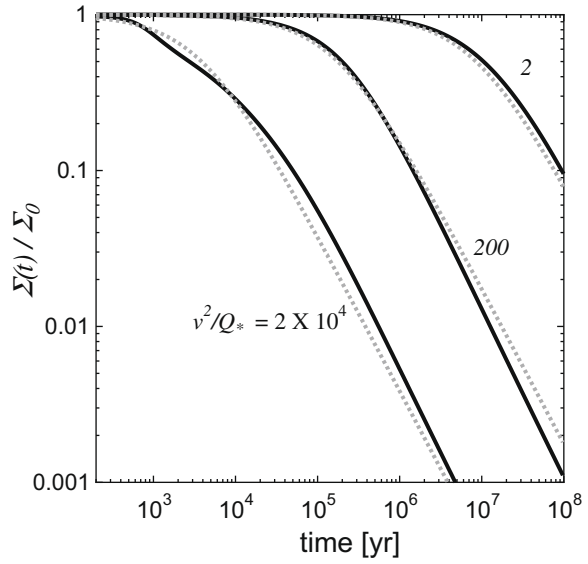

Fig. 8. Total mass of bodies as a function of time. The solid lines indicate the results on the numerical integration with $v^2/Q_D^\star = 2$–2×10^4 and the dot gray lines indicate Eq. (28).

Eq. (28) has the same form as previous studies (e.g., Dominik and Decin, 2003; Wyatt et al., 2007) but there is some difference in the mass depletion time. In Fig. 7, we plot the mass depletion time as a function of the ratio $v^2/Q_D^\star$. For the comparison we also plot the depletion time obtained by Wyatt et al. (2007). They neglected the effect of cratering collisions in their derivation of the depletion time. Our mass depletion time is shorter than that by Wyatt et al. about by the factors 5–7 even for large $v^2/Q_D^\star$. This difference is explained by the effect of cratering collisions.

For the ratio $v^2/Q_D^\star \gg 1$, we can obtain a simple expression of the mass depletion time in the same way as the mass flux of Eq. (25) (see also Appendix A). Thus, we obtain

$$\tau_{dep} = \frac{36\, m_{max}^{\frac{1}{3}}}{\Sigma_0 h_0 \Omega_K} \left(\frac{v^2}{2Q_D^\star}\right)^{-\frac{5}{6}} \left[\left(-\ln\epsilon + \frac{1}{2-b}\right)s_1 + s_2 + s_3\right]^{-1}. \quad (30)$$

In Fig. 7, we also plot Eq. (30). For large $v^2/Q_D^\star$, Eq. (30) agrees well with the exact value obtained from Eq. (29). We find the insensitiveness of the depletion time on the parameters b and ϵ in Eq. (30), too. Note that τ_{dep} becomes longer within a factor of 2 due to uncertainty of fragmentation model as we will discuss in Section 7.

6. Numerical calculation

We also calculate the mass evolution of bodies due to collisional fragmentation by numerical simulations to check the analytical formula of the mass depletion time of Eq. (29) (or the validity of Eq. (27)). In the numerical simulation, using a set of discrete mass batches having the surface number density of bodies, we calculate the mass flux in Eq. (7) by summing over all mass bins and integrate Eq. (1) with the mass flux over time through the fourth order of Runge-Kutta method. We set the mass ratio between adjacent mass batches to be 2. We consider that the bodies with mass ranging from 1.0×10^{-5} g to 1.3×10^{22} g are distributed from 2 AU to 3 AU and that their densities are 3 g cm^{-3}. Their initial total mass is the earth mass $M_\oplus$ and hence the surface density $\Sigma_0 = 1.1$ g cm^{-2}. The initial mass distribution is the power-law with the index of -11/6.

Fig. 8 shows mass depletion in collision cascades obtained with our numerical simulations for various values of $v^2/Q_D^\star$. The surface density is constant for $t \ll \tau_{dep}$ and inversely proportional to t for $t \gg \tau_{dep}$. The formula Eq. (28) with τ_{dep} of Eq. (29) is in excellent agreement with results from the numerical calculations. It should be note that, for $v^2/Q_D^\star = 2 \times 10^4$, the numerical result slightly deviates from the analytical formula. This is caused by a wavy structure in the mass distribution caused by setting low-mass end in the numerical calculations (e.g., Krivov et al., 2006; Thébault and Augereau, 2007), which is not taken into account in the derivation of the analytical formula.

In Fig. 9, we show similar numerical results but for various set of (b, ϵ). We find that the mass depletion is insensitive to b and ϵ. Thus the mass depletion in collision cascades practically depends on only the total mass of ejecta m_e in the outcome model, as shown in the previous sections.

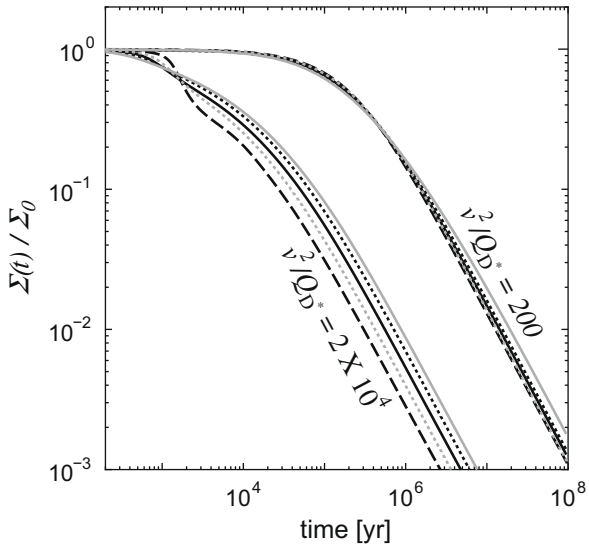

Fig. 9. Total mass evolution for $(b, \epsilon) = (5/3, 0.2)$ (solid line), (5/3, 0.01) (gray solid line), (5/3, 0.5) (gray dotted lines), (1.2, 0.2) (dashed lines), and (1.8, 0.2) (dotted lines) for $v^2/Q_D^\star = 200$ and 2×10^4.

7. Other fragmentation models

In Sections 4–6, we assumed that $v^2/Q_D^\star$ is independent of masses of colliding bodies in the collisional model and consider only the self-similar case. In general, however, the threshold value for catastrophic disruption, $Q_D^\star$, is dependent on the mass of the target (e.g. Holsapple, 1993; Benz and Asphaug, 1999) while collisional velocities v of small bodies have a very weak function of mass (e.g., Wetherill and Stewart, 1993; Inaba et al., 2003). According to Benz and Asphaug (1999), $Q_D^\star \propto m_1^{0.4-0.5}$ in the gravity regime and $Q_D^\star \propto m_1^{-0.1} - m_1^{-0.16}$ in the strength regime. Here we examine non-self-similar cases, assuming $v^2/Q_D^\star \propto m_1^{-p}$ in Eq. (8). We also assume that the ratio $v^2/Q_D^\star$ is much larger than unity in whole mass range of collision cascades. From the estimation of Eq. (14), we can say that this assumption is valid for a wide parameter range of collision cascades. Under the assumption of $v^2/Q_D^\star \gg 1$, we can neglect the contribution of collisions with $y \gtrsim 1$ and, fortunately, have an expression of the mass flux similar to Eq. (25), as described in Appendix A. That is, we obtain (see Appendix A for detail)

$$F(m) = -A^2\Omega_k h_0 m^{\frac{11}{3}-2\alpha-p(\alpha-1)}\left(\frac{v(m)^2}{2Q_D^\star(m)}\right)^{\alpha-1} \times\left[\left(-\ln\epsilon+\frac{1}{2-b}\right)s_1(\alpha)+s_2(\alpha)+s_3(\alpha)\right]. \quad (31)$$

Since $v^2/Q_D^\star \propto m^{-p}$, we have $11/3 - 2\alpha - p(\alpha-1) = 0$ for a steady state (i.e., $\partial F(m)/\partial m = 0$). Therefore, α is given by

$$\alpha = \frac{11+3p}{6+3p}. \quad (32)$$

O'Brien and Greenberg (2003) derived the same power-law exponent as Eq. (32), though they considered only the catastrophic collisions. In the same way, using Eqs. (31) and (32), we have

$$\tau_{dep} = \frac{m_{max}^{\frac{1}{3}}}{(2-\alpha)^2\Sigma_0 h_0\Omega_K}\left(\frac{v(m_{max})^2}{2Q_D^\star(m_{max})}\right)^{-\alpha+1} \times\left[\left(-\ln\epsilon+\frac{1}{2-b}\right)s_1(\alpha)+s_2(\alpha)+s_3(\alpha)\right]^{-1}. \quad (33)$$

Even in this non-self-similar case, the mass flux and the mass depletion time are not sensitive to the parameters ϵ and b in this non-self-similar case.

In the above derivation of Eq. (31), we used the power-law mass distribution of fragments in the outcome model described in Section 3. In Appendix B, we also derive a more general expression of $F(m)$ for arbitrary mass distribution of fragments, assuming that collisions with $y \ll 1$ are dominant. The mass flux is written in the form (see Appendix B for the detail derivation)

$$F(m) = -A^2\Omega_K h_0 m^{\frac{11}{3}-2\alpha-p(\alpha-1)}\left(\frac{v(m)^2}{2Q_D^\star(m)}\right)^{\alpha-1}\int_0^\infty d\phi\,\phi^{-\alpha} \times\{M_e(\phi)\ln M_m(\phi) - [1-M_e(\phi)]\ln[1-M_e(\phi)]\}, \quad (34)$$

where $M_e(\phi)$ is the total ejecta mass normalized by m_1 and $m_1 M_m(\phi)$ is the mean fragment mass in the ejecta defined by Eq. (B4).[2] The power-law exponent α of steady collision cascades is given by Eq. (32) in this general case, too. The detailed information of the mass distribution function is included only through the (normalized) mean fragment mass $M_m(\phi)$. However, the dependence of the flux on $M_m(\phi)$ is not sensitive because of its logarithmic dependence. Hence we again see in this general case that the mass flux is mainly determined by the total ejecta mass $M_e(\phi)$ in the collisional outcome.

[2] When we adopt the outcome model in Section 3, the mean fragment mass $m_1 M_m$ is obtained as $m_L e^{-1/(2-b)}$, and Eq. (34) reduces to Eq. (31).

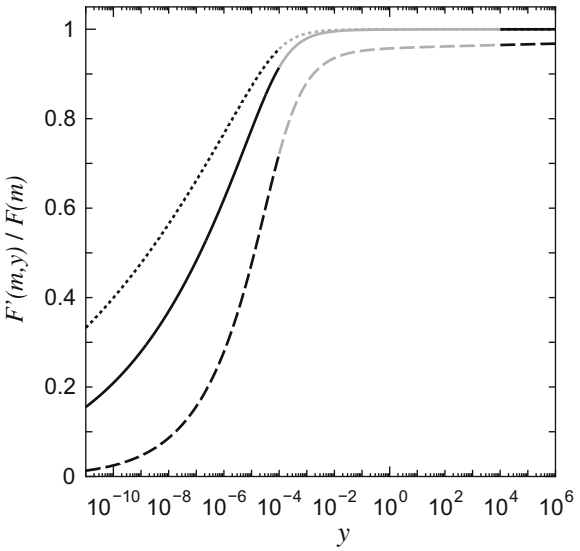

Fig. 10. Same as Fig. 5, but for non-self-similar cases. In the strength regime, $p = -0.12$ (dotted lines) and, in the gravity regime, $p = 0.45$ (dashed lines) while $p = 0$ in the self-similar case (solid line). Here the power-law index α of mass distribution of bodies is given by Eq. (32).

To see the contribution of cratering collisions in the mass flux of Eq. (31), we define $F'(m,y)$ in the same way as Eqs. (23) and (24) but using Eq. (31) and plot a similar figure to Fig. 5 in Fig. 10 for this non-self-similar collision cascades. We consider that $v^2/Q_D^\star$ is proportional to m_1^{-p} and that 20,000 at the mass m corresponding to the mass flux $F'(m,y)$ seen in Fig. 10. In the gravity regime with $p = 0.45$, the catastrophic collisions are more effective than the self-similar case. However, the cratering is still dominant compared with the catastrophic disruption in the gravity regime, too.

In addition, we also performed another numerical simulation for a more realistic $Q_D^\star$ to confirm the importance of the cratering.

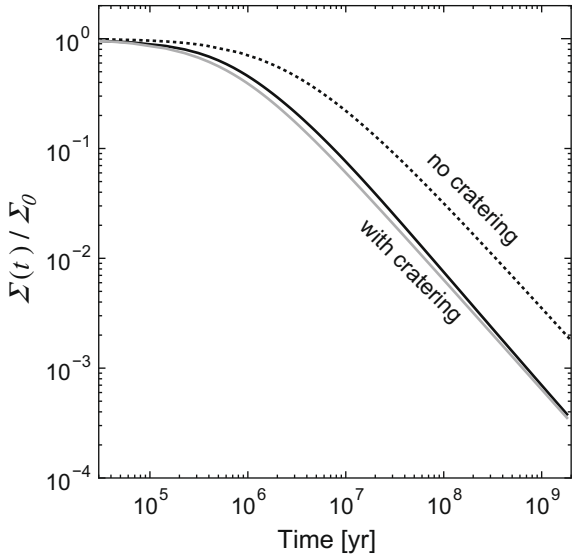

Fig. 11. Comparison of mass evolution with cratering (solid line) and that without cratering (dotted lines; neglecting collisions with $\phi < 1$) through numerical simulations. We chose $Q_D^\star = 3.5\times10^7(r_1/1\,\mathrm{cm})^{-0.38} + 0.3\,(\rho/1\,\mathrm{g\,cm^{-3}})(r_1/1\,\mathrm{cm})^{1.36}$ in erg/g for $v = 3$ km/s (Benz and Asphaug, 1999). The gray line indicates Eq. (28) with Eq. (33).

According to Benz and Asphaug (1999), we set $Q_D^\star = 3.5\times 10^7 (r_1/1\text{ cm})^{-0.38} + 0.3(\rho/1\text{ g cm}^{-3})(r_1/1\text{ cm})^{1.36}$ in erg/g. We consider $v = 3$km/s and that the other conditions are same as numerical simulations in Section 6. To see the effect of the cratering collisions, we perform two kinds of simulation. In the first case, we include both cratering and catastrophic collisions and, in second case, we take into account only the catastrophic collisions. In Fig. 11, we show the numerical results on the evolution of the total surface density of the collision cascade. The depletion time with cratering is 4–5 times shorter than that without cratering. The mass flux controls at high-mass end of the collision cascade and $Q_D^\star(m_{\max})$ is held by the gravity regime. Thus, this result is consistent with the analytical prediction for the gravity regime in Fig. 10. For $p = -0.12$-0 (the strength regime at the high-mass end), the depletion time is shortened by a factor 10–20 by cratering (see Fig. 10). Furthermore, Fig. 11 also shows that Eq. (33) is valid even in the case of the realistic $Q_D^\star$.

One may consider that the results on the effect of the cratering collisions are based on the collisional outcome model we set. In the fragmentation model of Section 3, we artificially set m_e as Eqs. (10) and the parameter ϕ is given by Eq. (8). Thus, for cratering collisions with $y \ll 1$ and $\phi \ll 1$, m_e is proportional to y (or the projectile mass) in Section 3 (and in the above general case, too). To charge this linear dependence of m_e on the projectile mass at cratering collisions, we redefine the parameter ϕ by $\phi = \left(v^2/2Q_D^\star\right)y^\xi/(1+y^\xi)$. Using this model, we calculate $F'(m,y)$ and plot the result in Fig. 12. The contribution of cratering collisions tend to decrease with ξ, because a collision with a small mass ratio yields the relatively small m_e for $\xi > 1$. This tendency is independent of ϵ and b. For large $\xi > 1.5$, the catastrophic collisions would be more important than the cratering. Nevertheless, according to the scaling law for cratering, the total ejecta mass (or the ejecta volume) is proportional to the mass of the projectile not only in the strength regime but also the gravity regime (see Eq. (21) and Table 2 of Holsapple (1993)). Laboratory experiments and hydrodynamic simulations on collisional dispersions also showed that the slope is close to unity (e.g., Housen et al., 1991; Benz and Asphaug, 1999). Thus we can say that the assumption $\xi \simeq 1$ is reasonable and that the case with $\xi > 1.5$ is not realistic. As a result, it is concluded that the cratering collisions make a dominate contribution to collision cascades in realistic outcome model.

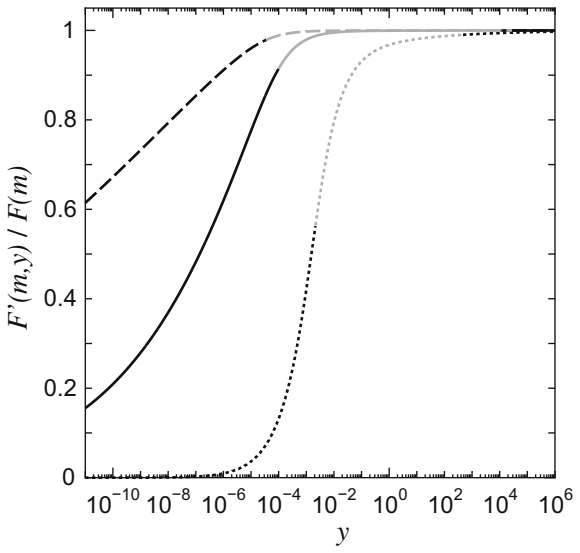

Fig. 12. Same as 5, but for $\xi = 1.5$ (dotted lines), 1 (solid line), and 0.9 (dashed lines). Here $\phi = \left(v^2/2Q_D^\star\right)y^\xi/(1+y^\xi)$ and $v^2/Q_D^\star = 2\times 10^4$.

Williams and Wetherill (1994) analytically compared the effect of cratering with catastrophic disruption. In their estimation, the ratio of the mass loss by cratering to that by catastrophic disruption is approximately given by $5\Gamma/\Gamma'$ in the high-velocity regime, where Γ is the ratio of the total ejecta mass at a single cratering to the projectile mass m_p and $\Gamma' m_p$ is the mass of the largest target that can be completely destroyed by a collision with the projectile. In the nominal case in their paper, the ratio Γ/Γ' is set to be 0.05, which makes cratering ineffective. This value seems too small, as explained below. In their model, near the transition from cratering to catastrophic, the ratio of the total ejecta mass to the target mass is given by Γ/Γ' for cratering while the ratio is equal to unity for catastrophic. If the total ejecta mass is continuous at the transition from cratering to catastrophic, the ratio Γ/Γ' should be unity. Most of the laboratory experiments and the hydrodynamic numerical simulations on collisional disruptions showed that the total ejecta mass continuously decreases at the transition from catastrophic to cratering (e.g., Housen et al., 1991; Takagi et al., 1984; Benz and Asphaug, 1999). Hence, we should set the ratio Γ/Γ' to be unity rather than 0.05 in a realistic collisional outcome model. If the ratio Γ/Γ' is set to be unity, cratering is more effective than catastrophic disruption in the estimation of Williams and Wetherill (1994), too. This is consistent with our result. It should be noted that laboratory experiments and hydrodynamic numerical simulations on collisional disruptions are not enough. New experiments and/or simulations may observe a jump in the ejecta mass near the transition. If such cases are found a lot, our result should be reconsidered. In addition, the contribution of cratering depends on our simple fragmentation model described in Section 3. When we apply other consistent fragmentation models with the laboratory experiences and fluid dynamical simulations on collisional dispersions, the contribution factor can change within a factor of 2.

8. Implication to planet formation

Debris disks are found around main-sequence stars. In the disk, In debris disks, the removable time of small dust by the radiation pressure is much shorter than the age of the central star. Therefore, the debris disk is fed by collisional fragments of planetesimals. The brightness of a debris disk is proportional to the total mass of the planetesimals. Therefore, the mass depletion time gives the evolution time of the brightness. Cratering collisions are important for the collisional evolution in debris disks. We derived the mass depletion time in Eq. (33), which is about four times shorter than that without cratering collisions when $Q_D^\star$ of largest bodies (planetesimals) is proportional to $m^{0.4} - m^{0.5}$ in the gravitational regime. Assuming the critical energy $Q_D^\star = Q_0(\rho/3\text{ g cm}^{-3})^{0.55}(m/10^{21}\text{ g})^{0.45}$ erg/g of planetesimals (Benz and Asphaug, 1999) and $v = e v_K$, we estimated the depletion time from Eq. (33) as

$$\tau_{\rm dep} = 4.0\times 10^8 \left(\frac{Q_0}{9.5\times 10^8\text{ erg/g}}\right)^{0.68}\left(\frac{m}{10^{21}\text{ g}}\right)^{0.64}\left(\frac{a}{50\text{ AU}}\right)^{0.18} \times \left(\frac{\Delta a/a}{0.1}\right)\left(\frac{e}{0.1}\right)^{-1.4}\left(\frac{\rho}{3\text{ g cm}^{-3}}\right)^{0.89}\left(\frac{M_{\rm tot}}{M_\oplus}\right)^{-1}\text{yr}, \quad (35)$$

where $M_{\rm tot}$ is the total mass of bodies in the ring-like debris disks with the width Δa at the distance a from the central star, and $M_\oplus = 5.97\times 10^{27}$ g is the Earth mass. This results is important for analysis of debris disks because the depletion time is related to the masses and the velocities of planetesimals. We should recall that $\tau_{\rm dep}$ of Eqs. (33) and (35) is the depletion time for the initial surface density. To estimate the evolution time of the depleted disks, we need to replace $\Sigma(t)$ or $M_{\rm tot}(t)$ in Eqs. (33) and (35).

Planets are formed by collisional accretion of planetesimals. Planetary embryos are formed through a runaway accretion of

planetesimals. The embryos do not collide each other in the oligarchic stage. In this stage, their growth slows down because of the enhancement of random velocities of planetesimals due to the perturbation by embryos themselves. The growth time of the embryo with mass M and semimajor axis a is given by (e.g., Tanaka and Ida, 1999; Kokubo and Ida, 2002)

$$\tau_{\rm grow} = 2.9\times10^6\left(\frac{m}{10^{21}\ {\rm g}}\right)^{1/9}\left(\frac{a}{1\ {\rm AU}}\right)^{1/6}\left(\frac{\rho_{\rm gas}}{10^{-9}\ {\rm g\ cm^{-3}}}\right)^{-1/3}\times\left(\frac{\rho}{3\ {\rm g\ cm^{-3}}}\right)^{5/9}\left(\frac{M}{10^{26}\ {\rm g}}\right)^{1/3}\left(\frac{\Sigma}{2.5\ {\rm g\ cm^{-2}}}\right)^{-1}{\rm yr}, \quad (36)$$

where m is the planetesimal mass, Σ is the surface density of the solid materials, and $\rho_{\rm gas}$ is the nebula density. On the other hand, total mass of planetesimals depletes by mutual collisions between planetesimals if their collisional energies per unit mass exceed the critical energy $Q_{\rm D}^\star$. We can apply Eq. (33) to the depletion time of the planetesimals. Inserting the relative velocity v determined by the equilibrium between the viscus stirring by embryos and the gas drag (Tanaka and Ida, 1999) and the critical energy $Q_{\rm D}^\star = Q_0(\rho/3\ {\rm g\ cm^{-3}})^{0.55}(m/10^{21}\ {\rm g})^{0.45}$ erg/g of planetesimals (Benz and Asphaug, 1999), we have

$$\tau_{\rm dep} = 8.9\times10^6\left(\frac{Q_0}{9.5\times10^8\ {\rm erg/g}}\right)^{0.69}\left(\frac{a}{5.2\ {\rm AU}}\right)^{2.4}\left(\frac{\rho_{\rm gas}}{10^{-9}\ {\rm g\ cm^{-3}}}\right)^{0.23}\times\left(\frac{m}{10^{21}\ {\rm g}}\right)^{0.57}\left(\frac{M}{10^{26}\ {\rm g}}\right)^{-0.46}\left(\frac{\rho}{3\ {\rm g\ cm^{-3}}}\right)^{0.89}\left(\frac{\Sigma}{2.5\ {\rm g\ cm^{-2}}}\right)^{-1}{\rm yr}. \quad (37)$$

In Fig. 13, we plot the growth time and the depletion time as functions of the embryo mass. When the planetary embryos are small enough, the growth time is much shorter than the depletion time. Then, embryos can grow more prior to the depletion. When the mass of embryos attains to an critical mass at which $\tau_{\rm grow} \simeq \tau_{\rm dep}$, the depletion of planetesimals would stop the growth of embryos (Inaba et al., 2003; Kenyon and Bromley, 2008). The critical mass of embryos at which $\tau_{\rm grow} = \tau_{\rm dep}$ is given by

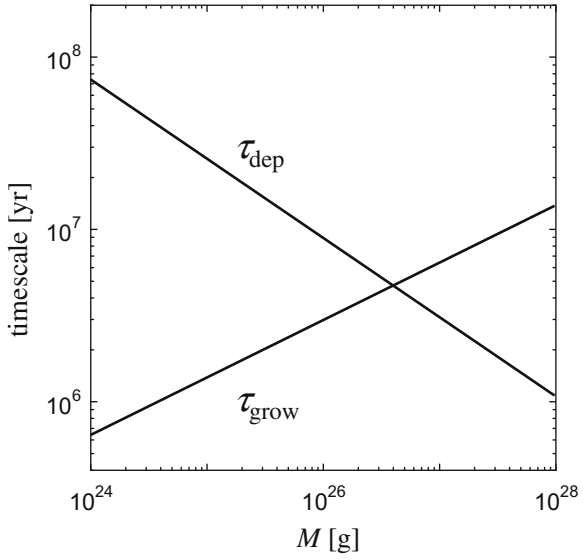

Fig. 13. The embryo growth time $\tau_{\rm grow}$ of Eq. (36) and the planetesimal depletion time $\tau_{\rm dep}$ of Eq. (37) as a function of the embryo mass M.

$$M = 6.7\times10^{-2}\left(\frac{Q_0}{9.5\times10^8\ {\rm erg/g}}\right)^{0.87}\left(\frac{m}{10^{21}\ {\rm g}}\right)^{0.58}\times\left(\frac{a}{5.2\ {\rm AU}}\right)^{2.8}\left(\frac{\rho_{\rm gas}}{10^{-9}\ {\rm g\ cm^{-3}}}\right)^{0.71}\left(\frac{\rho}{3\ {\rm g\ cm^{-3}}}\right)^{0.42}M_\oplus. \quad (38)$$

Eq. (38) shows that the critical mass of planetary embryos is comparable to the Mars mass. The semimajor axes of embryos are changed by migration (e.g., Ida and Lin, 2004, 2008; Nagasawa et al., 2007; Gomes et al., 2005) and the embryos further grow through collisions with other embryos for the long time orbital instability after gas depletion of protoplanetary disk (Chambers et al., 1996; Iwasaki and Ohtsuki, 2006). The critical mass in Eq. (38) is too small for embryos to start the gas capture for giant planet formation prior to the gas depletion (e.g., Ikoma et al., 2001). Note that this critical mass of embryos is independent of the surface density of planetesimals since both timescale is inversely proportional to Σ. To increase the critical mass of embryos to the earth mass, we would need large planetesimals with $\sim10^{23}$ g. Furthermore, the enhancement in collisional cross sections of embryos by their envelope makes their growth time shorter (e.g., Inaba and Ikoma, 2003; Inaba et al., 2003) and would also increase their critical mass. If $Q_{\rm D}^\star$ is larger than that we adopt from Benz and Asphaug (1999) for large planetesimals, it would also assist the growth of embryos. However, this estimate would be too simple because both the growth time and the depletion time become longer with the surface density decreasing and because the growth time may be shorter by the planetesimals and fragments having mass spectrum (Kenyon and Bromley, 2009). More detailed investigation on disruption and depletion of planetesimals are needed to clarify the planet formation process.

9. Summary

1. We construct a simple fragmentation model described in Section 3, which is reasonably consistent with laboratory experiments, scaling laws, and hydrodynamical simulations on collisional dispersions. Ignoring coalescence of colliding bodies for high collisional velocities, the fragmentation model is applied to the mass flux which Tanaka et al. (1996) developed for analysis of self similar collision cascades ($Q_{\rm D}^\star$ and v^2 is independent of mass). That clarifies the fragmentation model dependence. Furthermore, we expand the analysis to adapt in the case of $v^2/Q_{\rm D}^\star$ having a power-law dependence on mass.
2. Cratering collisions are dominant to the mass depletion (see Figs. 5, 10, and 12), because cratering collisions occur more frequently than catastrophic ones. This result does not depend on the outcome model of collisional disruption as long as we use realistic model (see Section 7). The depletion time depending on $v^2/Q_{\rm D}^\star \propto m^{-p}$ at high-mass end is reduced by a factor 4–5 for $p = 0.45$ (gravity regime) and 10–20 for $p = -0.12 - 0$ (strength regime) by taking into account the cratering collisions, where we assume $v^2/Q_{\rm D}^\star \propto m^{-p}$. Although Williams and Wetherill (1994) obtained a conclusion that cratering was negligible under the assumption that the total ejecta mass produced by one dispersion has a discontinuous transition between cratering and catastrophic disruption, our result is consistent with their analysis for a continuous dependence at transition from cratering to catastrophic as seen in collisional experiments (see Section 7).
3. We analytically derived the mass flux and the depletion time (Eqs. (31) and (33)) due to collisions for large $v^2/Q_{\rm D}^\star$, using the outcome model in Section 3. The assumption of large $v^2/Q_{\rm D}^\star$ is valid for a wide parameter range of collision cascades (see Eq. (14)).

4. Eq. (33) explicitly show the depletion time of collision cascades is mainly determined by the total ejecta mass of the outcome model (or the ratio $v^2/Q_D^\star$ at the high-mass end) and insensitive to the detail of the mass distribution of fragments in the outcome model (i.e., the power-law exponent and the mass of the largest fragments) as long as we consider realistic models. This result is confirmed by the more general expression of Eq. (34).
5. We confirm the power-law index (Eq. (32)) of mass distribution for $v^2/Q_D^\star \propto m^{-p}$ derived by O'Brien and Greenberg (2003) taking into account only catastrophic collisions and show the index remains valid for any fragment model including cratering in the high impact velocity regime (see Section 7 and Appendix B).
6. We applied the obtained expression of the depletion time to the planet formation process. We find that when the planetary embryos grow to a critical mass, their growth is suppressed by the depressed by the depletion of planetesimals due to collisional disruption. The critical mass given by Eq. (38) is comparable to the Mars mass (the Earth mass) for planetesimals with 10^{21} g (10^{23} g). This result suggests that the collisional disruption of planetesimals may be a crucial factor in the gas giant formation via core accretion.

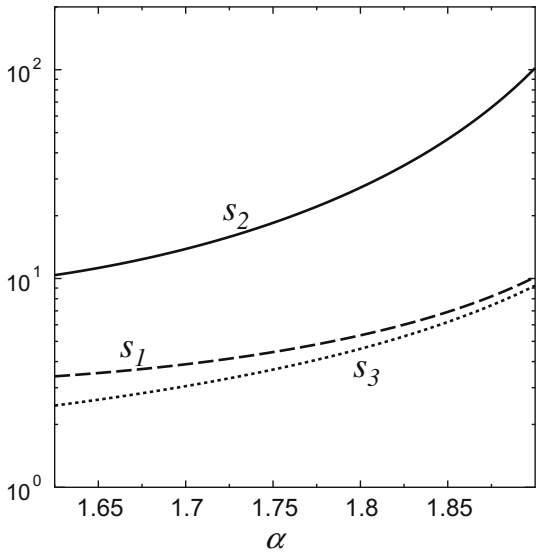

Fig. 14. $s_1(\alpha)$, $s_2(\alpha)$, and $s_3(\alpha)$ in Eqs. (A3)–(A5).

Acknowledgments

We are grateful to K. Wada, H. Genda, A. Krivov, and T. Löhne for helpful comments and discussions. We also thank D. O'Brien and S. Kenyon for critical comments which helped us improve the original manuscript.

Appendix A. Integration in F and τ_{dep} for large $v^2/Q_D^\star$

The mass flux of Eqs. (21) and (22) and the depletion time of Eq. (29) include integrals

$$\int_0^\infty dy \frac{y^{-\alpha}\left(1+y^{\frac{1}{3}}\right)^2\phi(y)}{1+\phi(y)}\left[-\ln\frac{\epsilon\phi(y)}{[1+\phi(y)]^2}+\frac{1}{2-b}\right] + \int_0^\infty dy \frac{y^{-\alpha}\left(1+y^{\frac{1}{3}}\right)^2}{1+\phi(y)}\ln(1+\phi(y)). \tag{A1}$$

In the case of $v^2/Q_D^\star \gg 1$, these integrals can be simplified, as explained below. The mass depletion is mostly governed by cratering collisions and the catastrophic collisions have a (minor) contribution only for $\phi(y) \sim 1$ (see Fig. 5). Hence, we can assume that $y \ll 1$ in the integrals for large $v^2/Q_D^\star$. Replacing $(1+y^{1/3})^2$ and $1+y$ by 1, and transforming the variable of the integration from y to ϕ, we can rewrite Eq. (A1) as

$$\left(\frac{v^2}{2Q_D^\star}\right)^{\alpha-1}\int_0^\infty d\phi\left\{\frac{\phi^{1-\alpha}}{1+\phi}\left[-\ln\frac{\epsilon\phi}{(1+\phi)^2}+\frac{1}{2-b}\right]+\frac{\phi^{-\alpha}}{1+\phi}\ln(1+\phi)\right\} = \left(\frac{v^2}{2Q_D^\star}\right)^{\alpha-1}\left[\left(-\ln\epsilon+\frac{1}{2-b}\right)s_1(\alpha)+s_2(\alpha)+s_3(\alpha)\right], \tag{A2}$$

where

$$s_1(\alpha) = \int_0^\infty d\phi \frac{\phi^{1-\alpha}}{1+\phi}, \tag{A3}$$

$$s_2(\alpha) = -\int_0^\infty d\phi \frac{\phi^{1-\alpha}}{1+\phi}\ln\frac{\phi}{(1+\phi)^2}, \tag{A4}$$

$$s_3(\alpha) = -\int_0^\infty d\phi \frac{\phi^{-\alpha}}{1+\phi}\ln(1+\phi). \tag{A5}$$

In Fig. 14, we show the values of the integrals $s_1(\alpha)$, $s_2(\alpha)$, and $s_3(\alpha)$. In self-similar collision cascade (i.e., $\alpha = 11/6$), $s_1 \simeq 6.3$, $s_2 \simeq 38.1$, and $s_3 \simeq 5.6$.

In the derivation of Eqs. (21) and (22) (or (29)), we assumed a constant $v^2/Q_D^\star$ and the self-similarity for the function f (Eq. (15)) and $\alpha = 11/6$. Hence this derivation seems to be invalid in the case of non-constant $v^2/Q_D^\star$. However, when the ratio $v^2/Q_D^\star$ is proportional to a power of the target mass, m_1, we can have an expression of the mass flux (the depletion time) similar to Eq. (25) (Eq. (30)) as long as $v^2/Q_D^\star \gg 1$, as shown below. As a result we will obtain Eq. (31).

We assume that $v^2/Q_D^\star \propto m^{-p}$ in Eq. (8). Also assuming that $y \ll 1$, we have $\phi = y v(m_1)^2/2Q_D^\star(m_1)$. In this case ϕ is dependent on m_1 (or x) as well as y. In the derivation of Eqs. (19) and (20) from (16), we changed the order of integration and integrated with respect to x first. Here, we cannot do that because of the x-dependence of ϕ. Nevertheless, if we transform the variable of the integrations from y to ϕ in Eq. (16), then, we can change the order of integration between ϕ and x. In the integrals with respect to x of Eqs. (19) and (20), the factors $x^{2\alpha-14/3}$ are all replaced by $x^{2\alpha-14/3+p(\alpha-1)}$ at the transformation of variable. Noting that Eq. (32) should be used instead of $\alpha = 11/6$ in this case, we have the same integrations with respect to x as in the derivation of Eqs. (21) and (22). As a result, we obtain the same result as Eq. (A2). It should be noticed that the constant $v^2/Q_D^\star$ in Eq. (A2) is replaced by $v(m)^2/Q_D^\star(m)$. Finally, leaving the m-dependence of $F(m)$, we obtain Eq. (31).

Appendix B. More general formula for the mass flux

In Appendix A, we obtained a simple formula for the mass flux, assuming that the contribution of the collisions with $y \ll 1$ is dominant in the case of $v^2/Q_D^\star \gg 1$, and using the outcome model in Section 3. Here, we derive a more general formula for the mass flux, adopting the similar assumption but using a more general outcome model than in Section 3.

In the more general case, we use the normalized impact energy $\phi(y)$ as well as in Section 3 but we only assume for the mass distribution of the ejecta at each collision

$$f_{\rm eject}(m, m_1, m_2) = f_{\rm eject}(x, \phi(y)) \tag{B1}$$

instead of Eq. (12), where $x = m/m_1$. That is, we seek a general expression of $F(m)$ for arbitrary mass distribution function of fragments with is parameterized by ϕ.

From Eq. (B1), the total ejecta mass $m_e(\phi)$ is equal to $m_1 f_{\rm eject}(1, \phi(y))$ and, using this m_e, $f_{\rm rem}$ is given by Eq. (13) in this case, too. Assuming $y \ll 1$, we put $\phi = y v^2/2Q_D^\star$ and also assume $v^2/Q_D^\star \propto m_1^{-p}$ as in Appendix A. Thus $\phi \propto m_1^{-p}$, too. Under these assumptions, transforming the variable from y to ϕ in Eq. (16) and changing the order of integration, we obtain

$$F(m) = -A^2 \Omega_K h_0 m^{\frac{11}{3}-2\alpha-p(\alpha-1)} \left(\frac{v(m)^2}{2Q_D(m)^\star}\right)^{\alpha-1} \int_0^\infty d\phi \phi^{-\alpha} \times \left\{ \int_0^1 dx x^{2\alpha-\frac{14}{3}+p(\alpha-1)} f_{\rm eject}(x,\phi) + [1 - f_{\rm eject}(1,\phi)] \int_{1-f_{\rm eject}(1,\phi)}^1 dx x^{2\alpha-\frac{14}{3}+p(\alpha-1)} \right\}. \quad \text{(B2)}$$

In this expression, $F(m)$ is proportional to $m^{11/3-2\alpha-p(\alpha-1)}$ as well as in Appendix A. Thus we again obtain Eq. (32) for steady state collision cascades. Using this and integrating by parts with respect to x, we finally obtain a general expression of the mass flux in steady collision cascades as

$$F(m) = -A^2 \Omega_K h_0 m^{\frac{11}{3}-2\alpha-p(\alpha-1)} \left(\frac{v(m)^2}{2Q_D^\star(m)}\right)^{\alpha-1} \int_0^\infty d\phi \phi^{-\alpha} \times \{M_e(\phi) \ln M_m(\phi) - [1 - M_e(\phi)] \ln[1 - M_e(\phi)]\}, \quad \text{(B3)}$$

where $M_e(\phi) = f_{\rm eject}(1, \phi(y))$ is the total ejecta mass normalized by m_1 and $m_1 M_m(\phi)$ is the mean fragment mass in the ejecta defined by

$$\ln M_m(\phi) = \frac{1}{M_e(\phi)} \int_0^1 dx \ln x \frac{df_{\rm eject}(x,\phi)}{dx}. \quad \text{(B4)}$$

Note that $df_{\rm eject}(x, \phi(y))/dx$ describes the differential mass distribution of fragments in the ejecta. It should be also noticed that $\ln M_m(\phi)$ and $\ln[1 - M_e(\phi)]$ are both negative since $M_m(\phi) < 1$ and $[1 - M_e(\phi)] < 1$. This expression is valid for arbitrary mass distribution of fragments with is parameterized by ϕ. When we adopt the outcome model in Section 3, the mean fragment mass m_1 M_m is obtained as $m_L e^{-1/(2-b)}$, and Eq. (B3) is reduced to Eq. (31).

References

Arakawa, M., 1999. Collisional disruption of ice by high-velocity impact. Icarus 142, 34–45.

Benz, W., Asphaug, E., 1999. Catastrophic disruptions revisited. Icarus 142, 5–20.

Bottke, W.F., Durda, D.D., Nesvorný, D., Jedicke, R., Morbidelli, A., Vokrouhlický, D., Levison, H.F., 2005. Linking the collisional history of the main asteroid belt to its dynamical excitation and depletion. Icarus 179, 63–94.

Chambers, J.E., Wetherill, G.W., Boss, A.P., 1996. The stability of multi-planet systems. Icarus 119, 261–268.

Dohnanyi, J.S., 1969. Collisional model of asteroids and their debris. J. Geophys. Res. 74, 2531–2554.

Dominik, C., Decin, G., 2003. Age dependence of the vega phenomenon: Theory. Astrophys. J. 598, 626–635.

Gomes, R., Levison, H.F., Tsiganis, K., Morbidelli, A., 2005. Origin of the cataclysmic Late Heavy Bombardment period of the terrestrial planets. Nature 435, 466–469.

Greenzweig, Y., Lissauer, J.J., 1992. Accretion rates of protoplanets. II. Gaussian distributions of planetesimal velocities. Icarus 100, 440–463.

Holsapple, K.A., 1993. The scaling of impact processes in planetary sciences. Ann. Rev. Earth Planet. Sci. 21, 333–373.

Housen, K.R., Schmidt, R.M., Holsapple, K.A., 1991. Laboratory simulations of large scale fragmentation events. Icarus 94, 180–190.

Ida, S., Lin, D.N.C., 2008. Toward a deterministic model of planetary formation. IV. Effects of type I migration. Astrophys. J. 673, 487–501.

Ida, S., Lin, D.N.C., 2004. Toward a deterministic model of planetary formation. I. A desert in the mass and semimajor axis distributions of extrasolar planets. Astrophys. J. 604, 388–413.

Ikoma, M., Emori, H., Nakazawa, K., 2001. Formation of giant planet in dense nebulae: Critical core mass revisited. Astrophys. J. 553, 999–1005.

Inaba, S., Tanaka, H., Nakazawa, K., Wetherill, G.W., Kokubo, E., 2001. High-accuracy statistical simulation of planetary accretion: II. Comparison with N-body simulation. Icarus 149, 235–250.

Inaba, S., Ikoma, M., 2003. Enhanced collisional growth of a protoplanet that has an atmosphere. Astron. Astrophys. 410, 711–723.

Inaba, S., Wetherill, G.W., Ikoma, M., 2003. Formation of gas giant planets: Core accretion models with fragmentation and planetary envelope. Icarus 166, 46–62.

Iwasaki, K., Ohtsuki, K., 2006. Orbital stability of protoplanetary systems in nebular gas and implications for terrestrial planet formation. Astron. J. 131, 3093–3099.

Kokubo, E., Ida, S., 2002. Formation of protoplanetary systems and diversity of planetary systems. Astrophys. J. 581, 666–680.

Kenyon, S.J., Bromley, B.C., 2002. Collisional cascades in planetesimal disks. I. Stellar flybys. Astron. J. 123, 1757–1775.

Kenyon, S.J., Bromley, B.C., 2004. Collisional cascades in planetesimal disks. II. Embedded planets. Astron. J. 127, 513–530.

Kenyon, S.J., Bromley, B.C., 2008. Variations on debris disks: Icy planet formation at 30–150 AU for 1–3 $M_\odot$ main-sequence stars. Astrophys. J. Suppl. Ser. 179, 451–483.

Kenyon, S.J., Bromley, B.C., 2009. Rapid formation of icy super-Earths and the cores of gas giant planets. Astrophys. J. 690, L140–L143.

Kenyon, S.J., Bromley, B.C., O'Brien, D.P., Davis, D.R., 2008. Formation and collisional evolution of Kuiper belt objects. In: Barucci, M.A., Boehnhardt, H., Cruikshank, D.P., Morbidelli, A. (Eds.), The Solar System beyond Neptune. University of Arizona Press, Tucson, pp. 293–313.

Kenyon, S.J., Luu, J.X., 1999. Accretion in the early outer Solar System. Astrophys. J. 526, 465–470.

Krivov, A.V., Löhne, T., Sremčević, M., 2006. Dust distributions in debris disks: Effects of gravity, radiation pressure and collisions. Astron. Astrophys. 455, 509–519.

Krivov, A.V., Sremčević, M., Spahn, F., 2005. Evolution of a Keplerian disk of colliding and fragmenting particles: A kinetic model with application to the Edgeworth Kuiper belt. Icarus 174, 105–134.

Krivov, A.V., Müller, S., Löhne, T., Mutschke, H., 2008. Collisional and thermal emission models of debris disks: Toward planetesimal population properties. Astrophys. J. 687, 608–622.

Löhne, T., Krivov, A.V., Rodmann, J., 2008. Long-term collisional evolution of debris disks. Astrophys. J. 673, 1123–1137.

Nagasawa, M., Thommes, E.W., Kenyon, S.J., Bromley, B.C., Lin, D.N.C., 2007. The diverse origins of terrestrial–planet systems. Protostars Planet. V, 639–654.

O'Brien, D.P.O., Greenberg, R., 2003. Steady-state size distributions for collisional populations: Analytical solution with size-dependent strength. Icarus 164, 334–345.

Paolicchi, P., Verlicchi, A., Cellino, A., 1996. An improved semi-empirical model of catastrophic impact processes. I. Theory and laboratory experiments. Icarus 121, 126–157.

Stern, S.A., Colwell, J.E., 1997. Collisional erosion in the primordial Edgeworth-Kuiper belt and the generation of the 30–50 AU Kuiper gap. Astrophys. J. 490, 879–882.

Tanaka, H., Ida, S., 1999. Growth of a migrating protoplanet. Icarus 139, 350–366.

Tanaka, H., Inaba, S., Nakazawa, K., 1996. Steady-state size distribution for the self-similar collision cascade. Icarus 123, 450–455.

Takagi, Y., Mizutani, H., Kawakami, S., 1984. Impact fragmentation experiments of basalts and pyrophyllites. Icarus 59, 462–477.

Thébault, P., Augereau, J.-C., 2007. Collisional processes and size distribution in spatially extended debris discs. Astron. Astrophys. 472, 169–185.

Wyatt, M.C., Smith, R., Greaves, J.S., Beichman, C.A., Bryden, G., Lisse, C.M., 2007. Transience of hot dust around Sun-like stars. Astrophys. J. 658, 569–583.

Wetherill, G.W., Stewart, G.R., 1993. Formation of planetary embryos: Effects of fragmentation, low relative velocity, and independent variation of eccentricity and inclination. Icarus 106, 190–209.

Williams, D.R., Wetherill, G.W., 1994. Size distribution of collisionally evolved asteroidal populations – Analytical solution for self-similar collision cascades. Icarus 107, 117–128.